Supporting Information

Directing the distribution of potassium cations in zeolite-LTL through crown ether addition

Hae Sung Cho[a,†], Adam R. Hill[b,†], Minhyung Cho[a], Keiichi Miyasaka[a], Kyungmin Jeong[a], Michael W. Anderson[b,*], Jeung Ku Kang[a,*] and Osamu Terasaki[a,c,d,*]

[a] Graduate School of Energy, Environment, Water, and Sustainability (EEWS), Korea Advanced Institute of Science and Technology (KAIST), Daejeon 34141, Republic of Korea

[b] Centre for Nanoporous Materials, School of Chemistry, The University of Manchester, Oxford Road, Manchester M13 9PL, United Kingdom

[c] Department of Materials and Environmental Chemistry, Stockholm University, Stockholm SE-10691, Sweden

[d] School of Physical Science and Technology, Shanghai Tech, 319 Yueyang Road, Shanghai 200031, China

[†]Contributed equally to this work

* Email: m.anderson@manchester.ac.uk, jeungku@kaist.ac.kr or terasaki@kaist.ac.kr

Experimental details

Materials

Zeolite-LTL frameworks with different amounts of CE molecules were synthesized following the synthesis procedure of Brent and Anderson [1] modified from the previous study [2]. The molar ratios for synthesis of the zeolite gel were 10.2 K_2O : 1 Al_2O_3 : 20 SiO_2 : 1030 H_2O : [0 – 4] 21-crown-7. Potassium hydroxide (KOH) and aluminum sulfate octadecahydrate ($Al_2(SO_4)_3 \cdot 18H_2O$) were dissolved in distilled water. The solution was stirred for 10 minutes until a homogeneous solution was obtained. A siliceous solution was prepared separately by adding Ludox (HS-40 colloidal silica) to distilled water. The silica solution was poured to the alumina solution with vigorous stirring. 21-crown-7 was then added to reactant solution, which is synthesized using a procedure by Ziafati *et al.* [3]. The mixture was then stirred for 18 h at room temperature by which time a turbid gel resulted. The resultant gel was then transferred into a Teflon lined stainless steel autoclave. After heating the autoclave at 453K for 3 days for all samples under a static condition, the reaction was quenched by plunging the autoclave into cold water. The resulting crystals were filtered with distilled water washing and dried at 383K overnight. The sample obtained in this manner is denoted as LTL-n. Here, 'n' indicates the 21-crown-7 molar fraction in the zeolite-LTL synthesis gel.

Electron microscopy

Scanning electron microscopic (SEM) images were taken by a JSM-7600F operated at 1 kV (accelerating voltage: 3 kV, specimen bias: 2 kV) and 3 mm of working distance. Powder samples were dispersed on a carbon pasted cupper support without any coating.

X-ray diffraction

Powder X-ray diffraction (XRD) measurements for zeolite-LTL with different amounts of CE were collected on BL02B2 at the synchrotron radiation facility SPring-8, Japan. A Debye-Scherrer type detector was used with an imaging plate at a wavelength of 0.099746 nm. Si fine powder (NIST SRM 640d) was used as the standard to calibrate wavelength. The powder sample was mounted in a fused soda capillary (diameter = 0.3

mm). The powder XRD patterns of sample were collected in a 2θ range of up to 76° (step = 0.01° and exposure time for each measurements = 30 min). *LeBail* and *Rietveld* refinements [4-5] of LTL zeolite with CE were performed using the JANA program [6] over the full sampled angular range based on P6/mmm SG for the LTL zeolite framework and P1 for the CE molecule. The Bragg peaks were modeled by a Pseudo-Voigt peak-shape function modified for asymmetry, with six refinable coefficients. The background was treated using a Legendre polynomial with six refinable parameters for the orthorhombic and monoclinic samples. The starting atomic coordinates for the zeolite-LTL frameworks were adopted from the previous studies [7 - 10] and starting positions for potassium cations were obtained from a difference Fourier analysis [11]. The initial atomic position of CE within the zeolite framework was obtained by computational simulation calculated using ZEBEDDE (zeolites by evolutionary de novo design). Occupancies for CE molecules were calculated using the molar ratios of CE molecules and zeolite-LTL unit cells, which were obtained from the TGA analysis. Because of the complexity of the structural model, constraints on Si-O, Al-O, C-C, C-O distances were applied. Their weight was totally removed in the final cycles. An isotropic atomic displacement parameter was imposed for individual atoms of K, Si, Al, O, and C.

Theoretical Details

Monte-Carlo simulations

CrystalGrower utilizes an interface with the program *ToposPro* that partitions crystal structure coordinates into the framework's natural tiling. These tiles are then used as *coarse-graining* building blocks in the *CrystalGrower* growth simulation process, and can be treated as metastable, rate-determining species. Coordination at tetrahedral atoms (T-atoms) can be denoted by its "Q" number e.g. Q^3 denotes the T-atom is coordinated to three other T-atoms, with one terminating OH group to compete the coordination of the tetrahedron. Three of these tiles can be considered as closed cages consisting entirely of Q^3 vertices: the cancrinite cage (*t-can)*, the double 6-ring (*t-hpr*), and the large supercage which forms the one-dimensional channels known as *t-lil*. The other

two small tiles consist of a combination of Q^2 and Q^3 vertices: *t-ste* and *t-kaa*. The *CrystalGrower* approach introduces taking the previously mentioned natural tiles / rate-determining elements and generating separate destabilization energy diagrams for each unit. Each level on these so-called 'energy ladders' corresponds to the loss of condensation from one tetrahedral atom in the unit e.g. changing from a Q^4 to a Q^3 site (and then if necessary to a Q^2 site). Combining these ladders with user-defined parameters such as supersaturation and temperature, probabilities can be assigned for the likelihood of certain units to grow. Incorporating a Monte-Carlo algorithm into this approach allows the accurate simulation of crystal growth from a medium with known conditions.

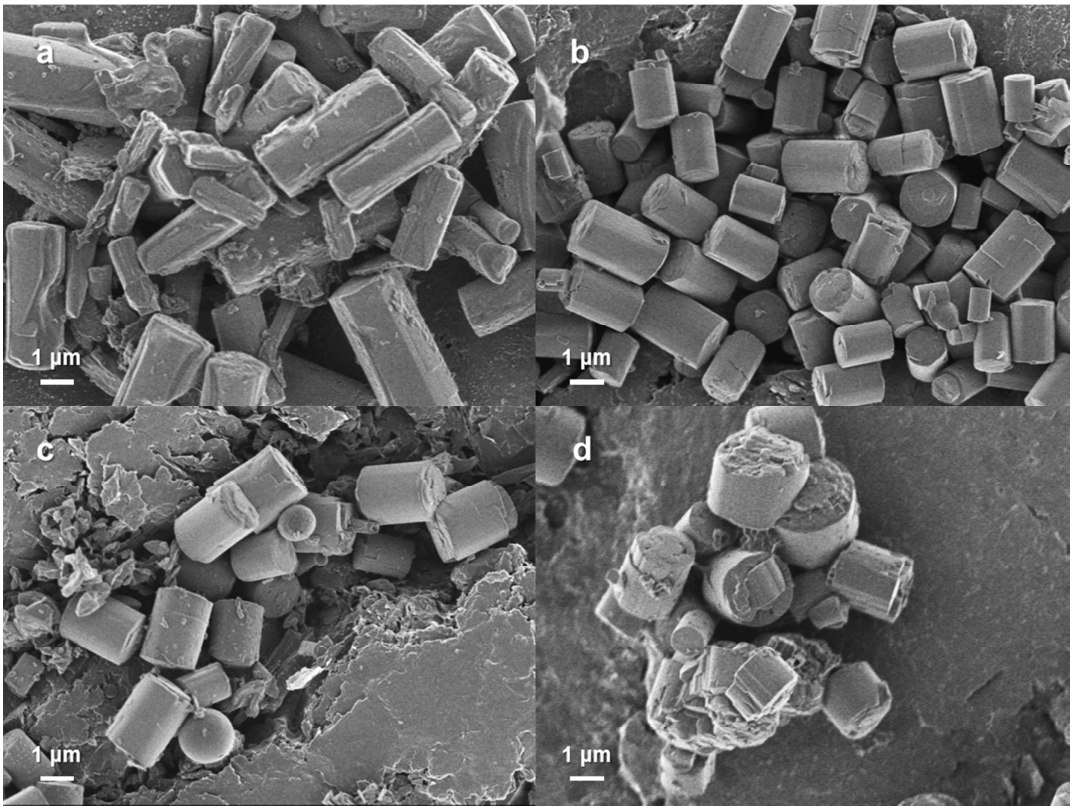

Figure S1. Low magnifided SEM micrographs of (a) LTL-0, (b) LTL-1, (c) LTL-2 and (d) LTL-4 showing overall morphology of zeolite-LTL particles.

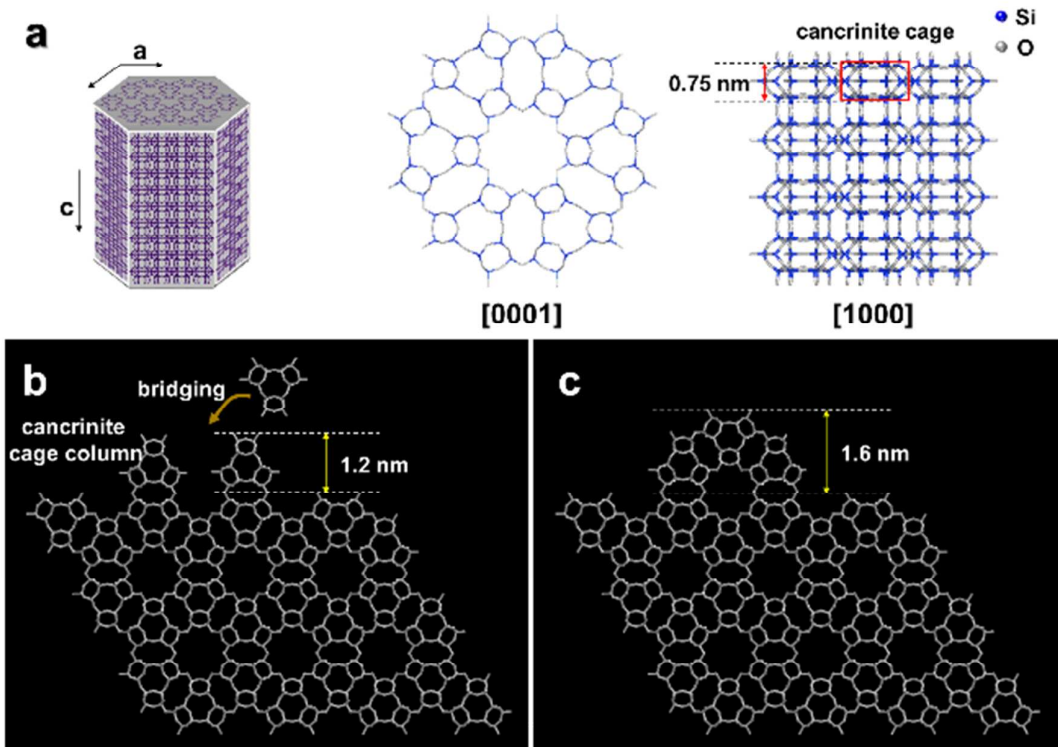

Figure S2. (a) 3D model of the zeolite-LTL framework structure and 2D displays along [0001] and [1000] direction. **(b)** Growth mechanism of zeolite-LTL before bridging cancrinite cage, and **(c)** after bridging cancrinite cage on (0001) surface.

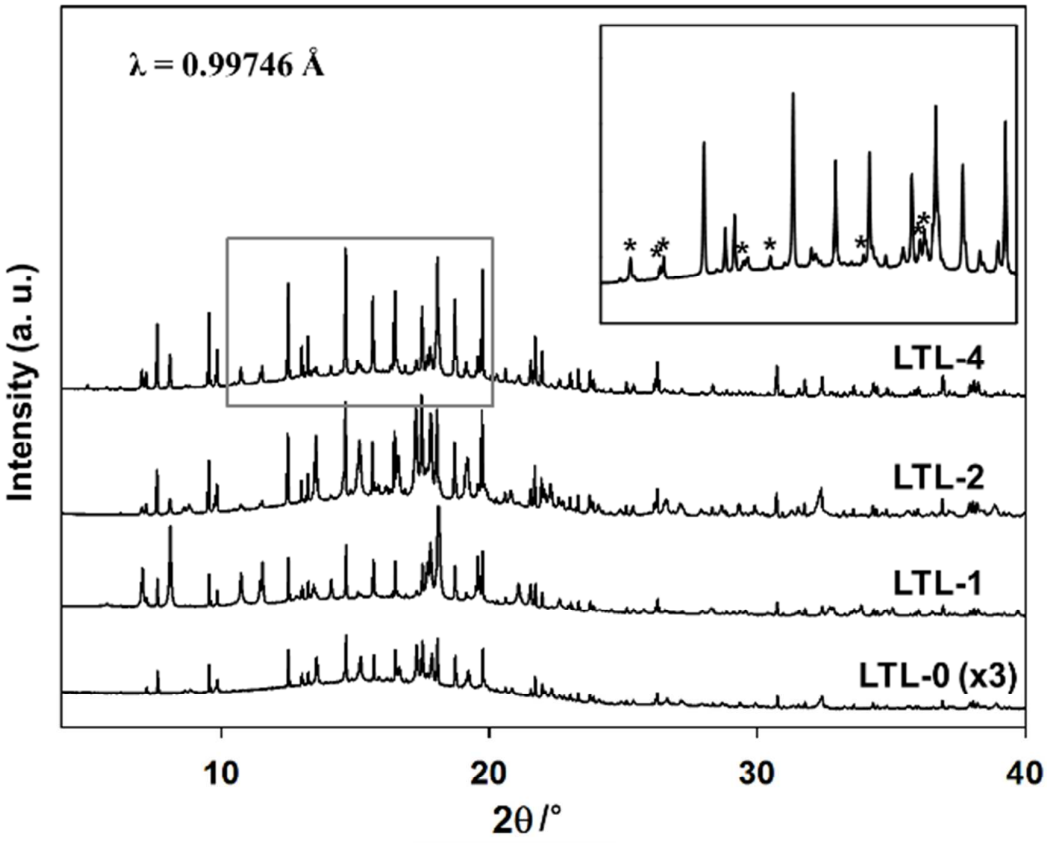

Figure S3. XRD patterns of zeolite-LTL with different amount of CE in the 2θ range from 4.0° to 40.0°. The reflections with star mark (*) indicates zeolite with a coexistence of MER framework structure, competitive phase of zeolite-LTL.

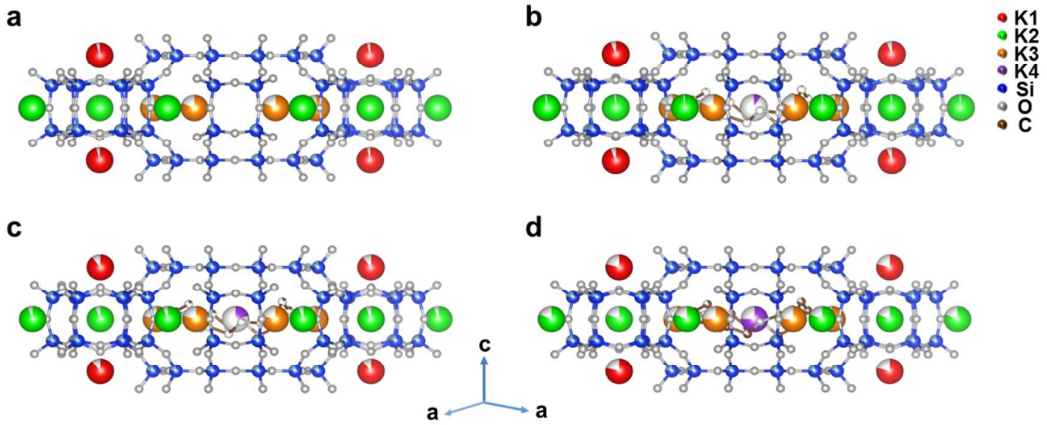

Figure S4. Configuration of potassium cation and CE molecule within the zeolite-LTL framework unit cell in the [1000] direction with different amount of CE: (a) LTL-0, (b) LTL-1, (c) LTL-2, (d) LTL-4. The occupancies of each atom are displayed as circle graphs.

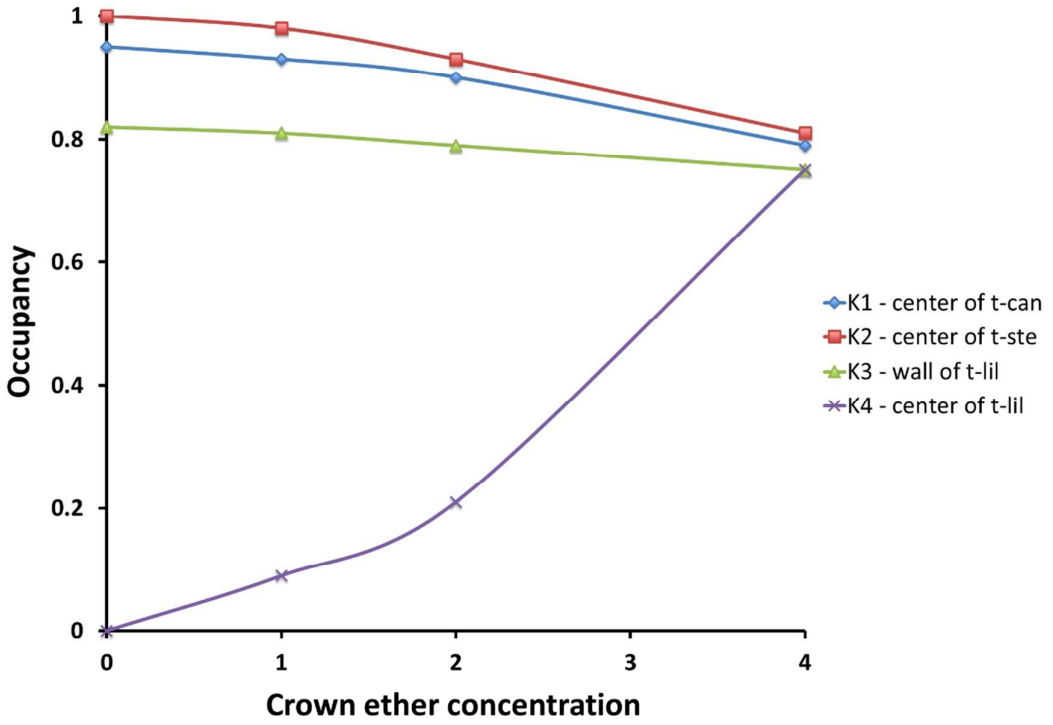

Figure S5. Graphical representation of the migration of potassium cations from positions K1, K2 and K3 (cation sites A, B and C) to position K4 (site F) as the concentration of CE is increased. The occupancy of K1 K2 and K3 decreases by a small amount, however their combined migration has a large effect on the occupancy of K4, indicating a clear preference for potassium to migrate to the center of the large pore cavity (*t-lil*) at higher CE concentrations.

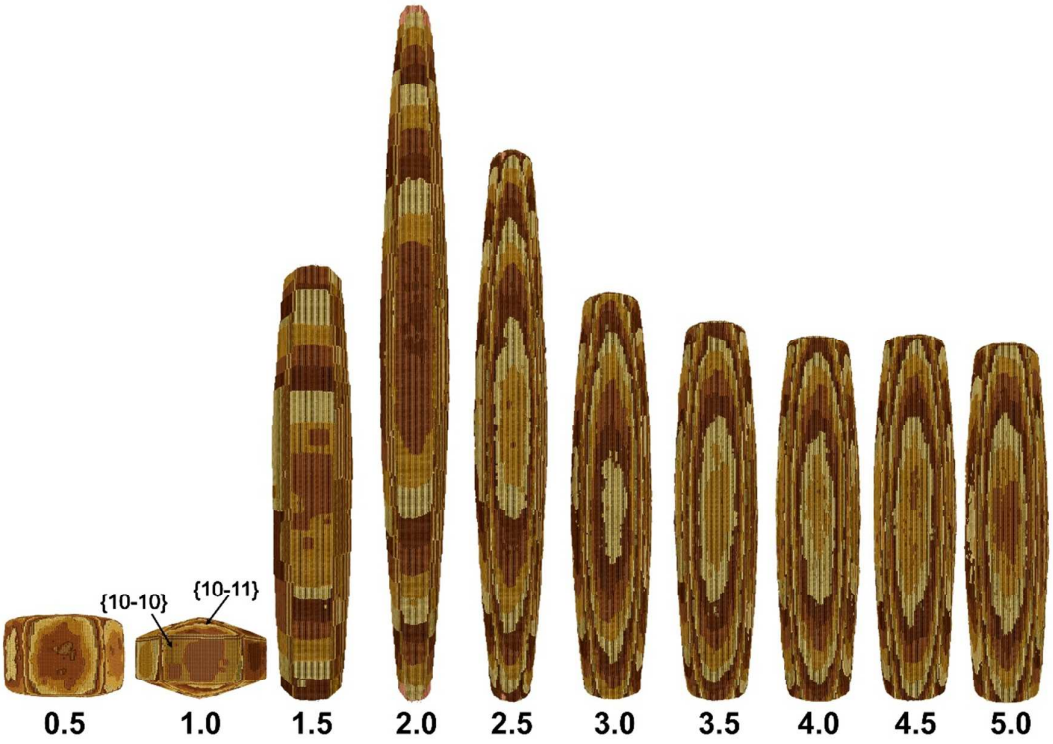

Figure S6. Simulation results of LTL crystals grown at equilibrium supersaturation. From Left to Right: Results from varying the condensation energy for *t-lil* from 0.5 kcal mol^{-1} to 5.0 kcal mol^{-1}. The side facets and diagonal-facing facets are labelled {10-10} and {10-11}, respectively. Basal {0001} facets are not labelled. Images were produced using the *CrystalGrower* visualization package.

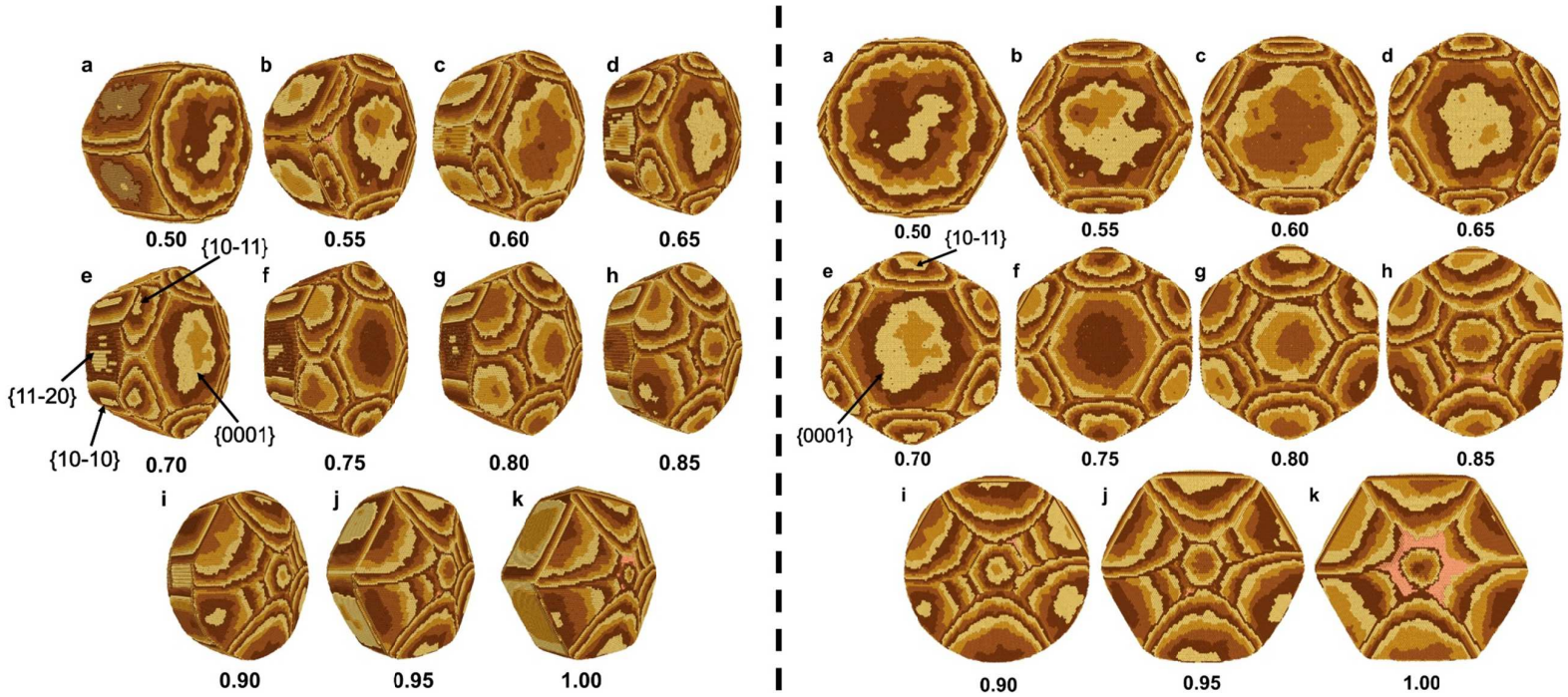

Figure S7. A detailed view of simulations where the destabilization energy for *t-lil* is varied between 0.50 and 1.00 kcal mol^{-1} with the energy increasing by 0.05 kcal mol^{-1} from a – k. Simulations performed at equilibrium supersaturation conditions. **Left:** A side on view of each tablet shaped crystal, with the end face of the crystal labelled as {0001}, along with the side facets labelled as {10-10}. Also shown are the diagonal facets {10-11} encroaching on the basal face and the additional side facets that are rotated by 30° giving the crystal a rounded look: {11-20}. **Right:** A top-down view of the same simulation results showing, the effect of the growth of these facets on the shape of the crystal. Images were produced using the *CrystalGrower* visualization package.

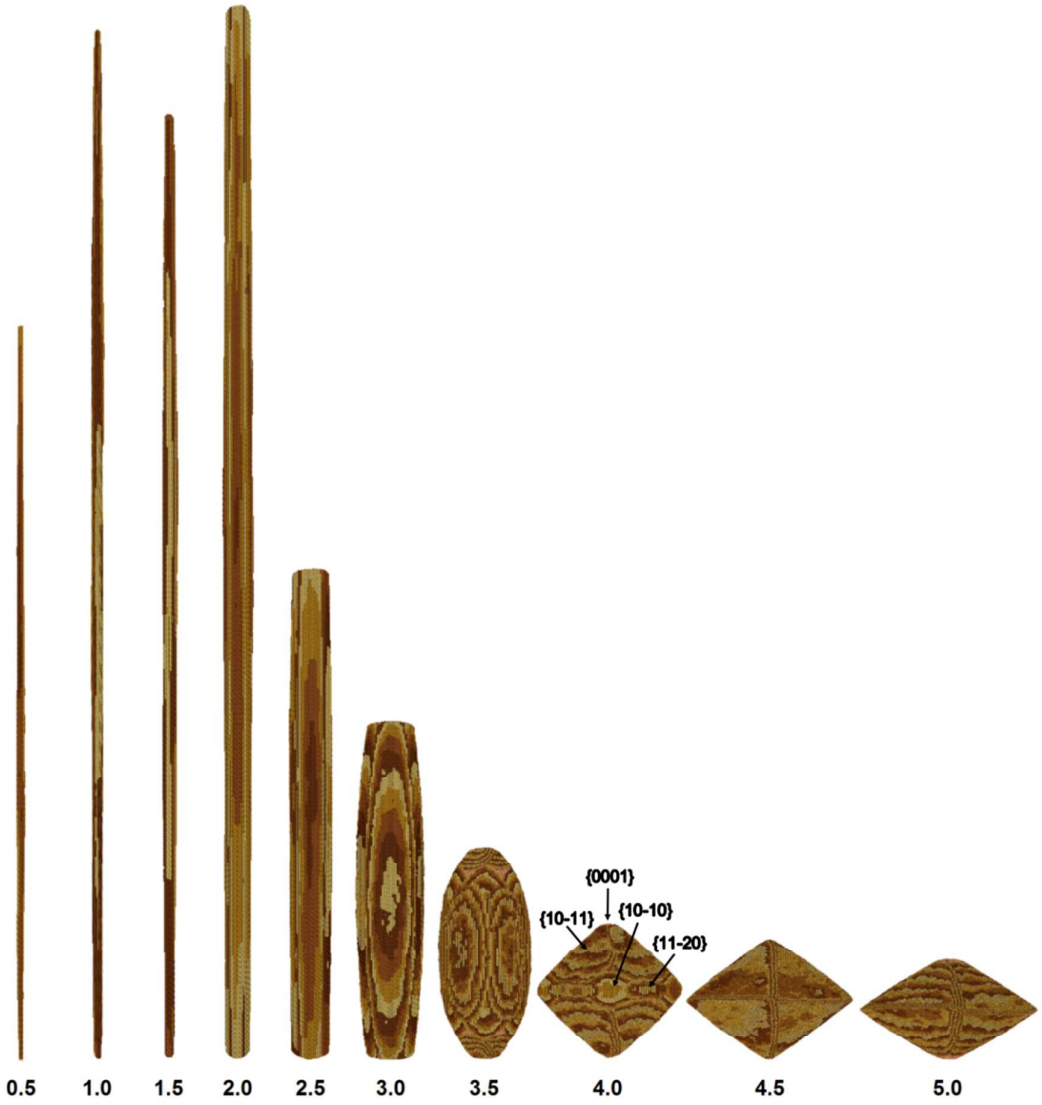

Figure S8. Simulation results of LTL crystals grown at equilibrium supersaturation. From Left to Right: Results from varying the condensation energy for *t-can* from 0.5 kcal mol^{-1} to 5.0 kcal mol^{-1}. The side facets, additional side facets rotated by 30°, and diagonal-facing facets are labelled {10-10}, {11-20} and {10-11}, respectively, along with the basal facets labelled {0001}. The simulations from 0.5 – 1.5 kcal mol^{-1} were restricted to 10% of the usual simulation length due to the limited size of the simulation box combined with the rapid growth of the crystal in the *z* direction. Images were produced using the *CrystalGrower* visualization package.

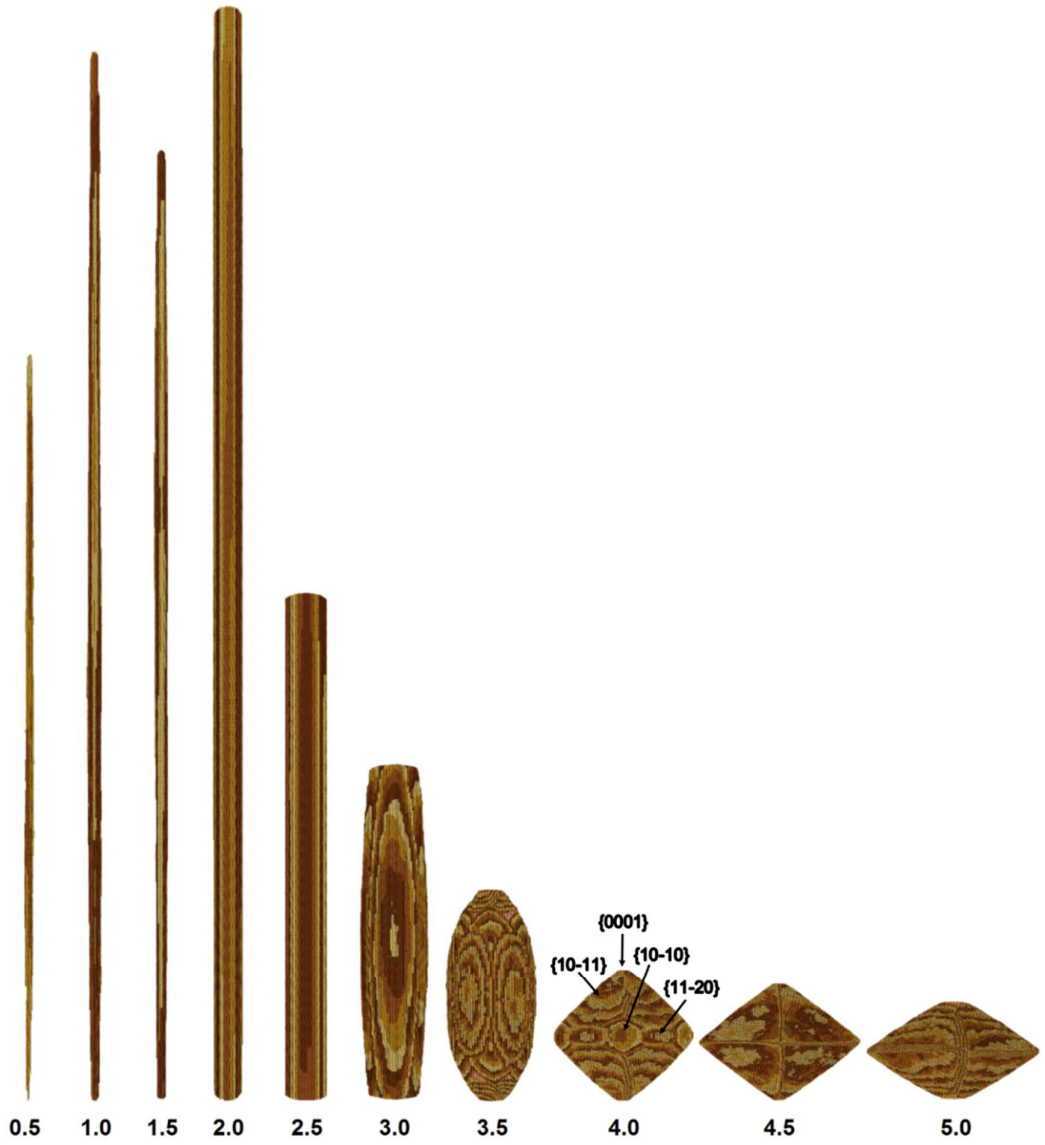

Figure S9. Simulation results of LTL crystals grown at supersaturation values of ~3 kcal mol^{-1}. From Left to Right: Results from varying the condensation energy for *t-can* from 0.5 kcal mol^{-1} to 5.0 kcal mol^{-1}. The side facets, additional side facets rotated by 30°, and diagonal-facing facets are labelled {10-10}, {11-20} and {10-11}, respectively, along with the basal facets labelled {0001}. The simulations from 0.5 – 1.5 kcal mol^{-1} were restricted to 10% of the usual simulation length due to the limited size of the simulation box combined with the rapid growth of the crystal in the *z* direction. Images were produced using the *CrystalGrower* visualization package.

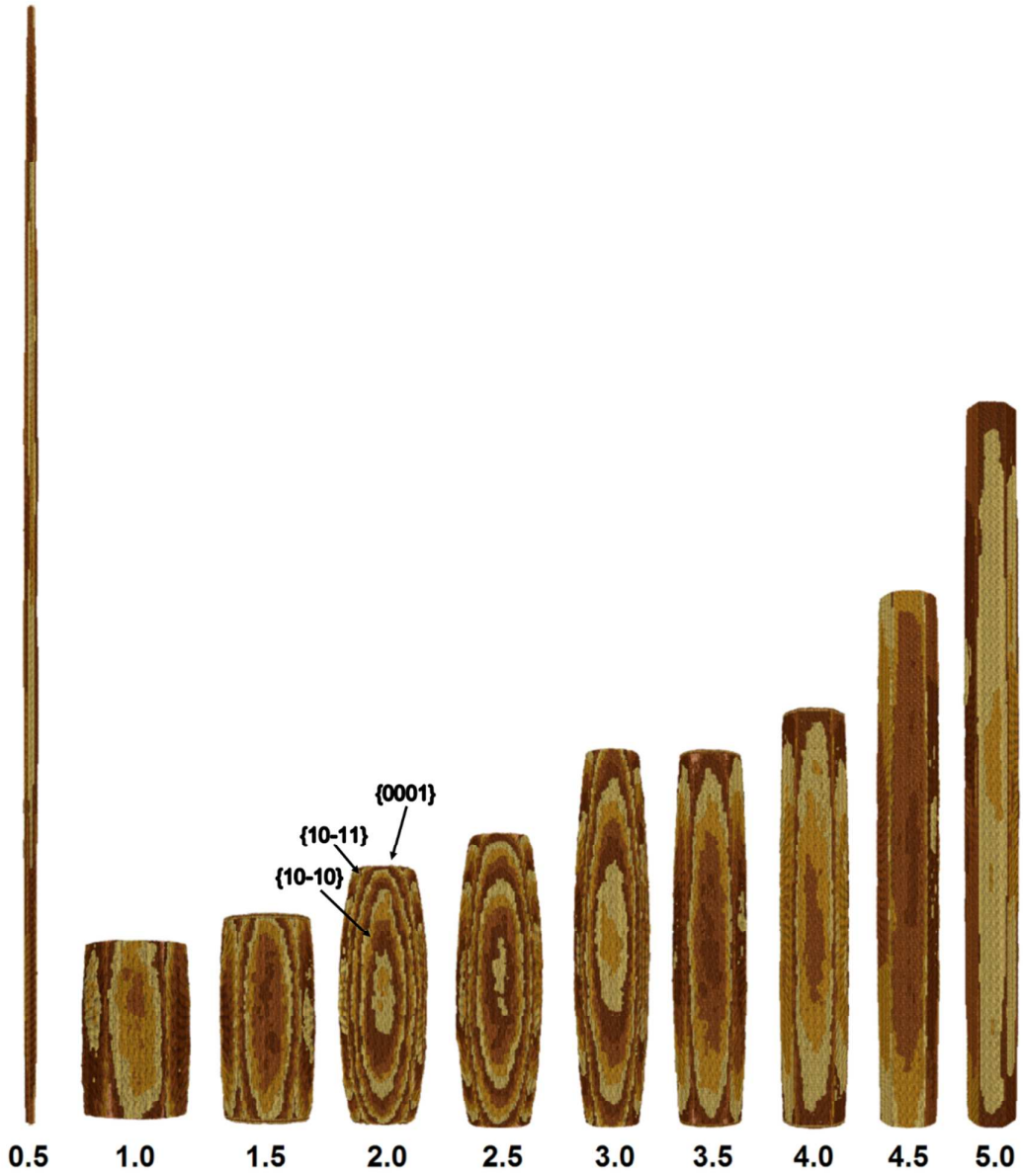

Figure S10. Simulation results of LTL crystals grown at equilibrium supersaturation. From Left to Right: Results from varying the condensation energy for *t-ste* from 0.5 kcal mol^{-1} to 5.0 kcal mol^{-1}. The side facets and diagonal-facing facets are labelled {10-10} and {10-11}, respectively, along with the basal facets labelled {0001}. The simulation at 0.5 kcal mol^{-1} was restricted to 10% of the usual simulation length due to the limited size of the simulation box combined with the rapid growth of the crystal in the *z*-direction. Images were produced using the *CrystalGrower* visualization package.

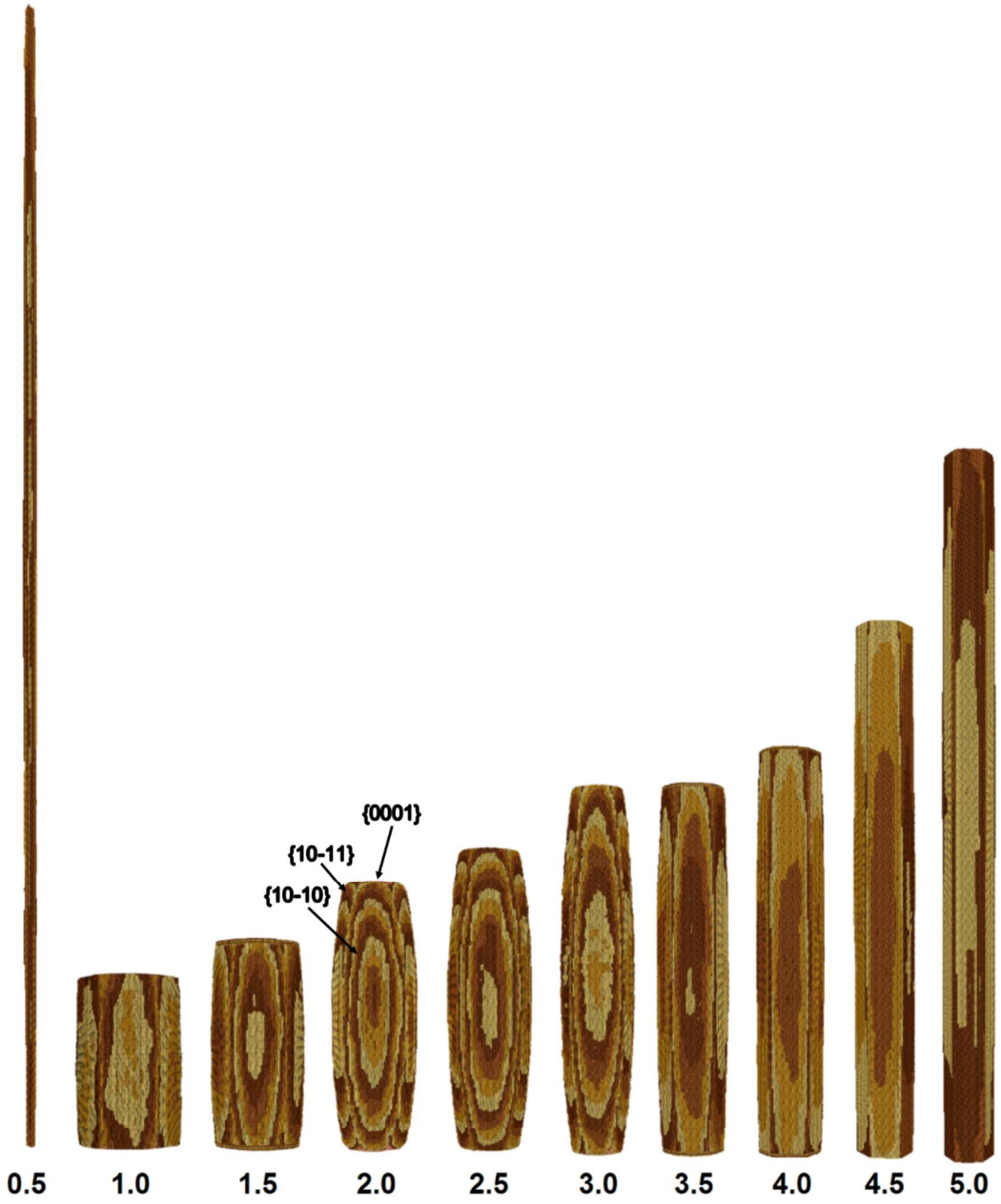

Figure S11. Simulation results of LTL crystals grown at supersaturation values of ~3 kcal mol^{-1}. From Left to Right: Results from varying the condensation energy for *t-ste* from 0.5 kcal mol^{-1} to 5.0 kcal mol^{-1}. The side facets and diagonal-facing facets are labelled {10-10} and {10-11}, respectively, along with the basal facets labelled {0001}. The simulation at 0.5 kcal mol^{-1} was restricted to 10% of the usual simulation length due to the limited size of the simulation box combined with the rapid growth of the crystal in the *z* direction. Images were produced using the *CrystalGrower* visualization package.

Discussion of Simulation Trends in Figures S8-S11.

The simulation results of changing the energy of the *t-can* cage (Figures S8 and S9), the trend in aspect ratio differs greatly to *t-lil*. At ≤ 2.0 kcal mol^{-1} the aspect ratio of the crystal increases dramatically, due to the low energy cost of growing single cancrinite columns *versus* cross-linking said columns. For energy values between 2.0 and 3.5 kcal mol^{-1} the crystal aspect ratio decreases, and the usual LTL crystal morphology of hexagonal prisms can be observed, with rounding at 3.5 kcal mol^{-1} due to the appearance of facets rotated 30° to the {10-10} side facets (these are {11-20} facets). At energy values of 4.0 kcal mol^{-1} and greater, the aspect ratio is decreased further to give crystals similar to the puck-shaped crystals observed at low energies (0.60 - 1.0 kcal mol^{-1}, Figures 4 and S7) for *t-lil*. The crystals grown at high *t-can* energies however, do not adopt as low an aspect ratio as those at low *t-lil* energies. They also exhibit much more pronounced {10-11} and {11-20} facets at the cost of the {0001} and {10-10} facets. For *t-ste* as shown in Figures S10 and S11, it can be observed that with increasing energy, generally, the aspect ratio of the crystal increases. The exception to this being the simulation result at 0.5 kcal mol^{-1} due to the tendency for the crystal to grow as columns of *t-ste* with minimal cross-linking caused by the energies of adjacent cages of different types being much higher. It is notable that the overall morphology of the crystal remains consistent with varying the energy of *t-ste*. The crystal retains its hexagonal prismatic shape exhibiting {0001} and {10-10} facets, with the appearance of some small {10-11} faces on the simulations between 2.0 and 3.5 kcal mol^{-1}. In addition, we find that these cage simulations exhibit the same differences as *t-lil* between simulations at equilibrium and supersaturated conditions, where the overall morphology is smoother at supersaturated conditions due to Ostwald Ripening.

Table S1. Crystal dimensions of LTL-n from SEM investigation [a]

Sample	Diameter (μm)	Length (μm)	Aspect ratio
LTL-0	1.4(1)	3.8(2)	2.7(1)
LTL-1	1.4(1)	1.9(3)	1.4(2)
LTL-2	1.3(2)	1.7(1)	1.3(2)
LTL-4	2.1(2)	1.6(2)	0.8(2)

a) Calculated the average from 10 zeolite-LTL particles. The standard deviations are shown in brackets. All products were synthesized at 453K for 3 d.

Table S2. Structural information for nucleation domain of LTL-n zeolite crystals [a]

Sample	Number of nucleation sites	Sum of area (nm^2)	Average nucleation area (nm^2)
LTL-0	1.6 (3)	103 (1)	64.4
LTL-1	4.8 (4)	126 (3)	26.3
LTL-2	12 (1)	152 (2)	12.7
LTL-4	19 (3)	226 (5)	11.9

a) Calculated the average from 10 zeolite-LTL particles. The standard deviations are shown in brackets.

Table S3. Atomic parameters resulting from the Rietveld refinement of LTL-0[a]

Atom	Occupancy	*x*	*y*	*z*	U_{iso} ($Å^2$)
Si1	0.7777	0.0876(6)	0.3447(3)	0.5	0.0152(3)
Si2	0.7777	0.1625(4)	0.4823(7)	0.2108(2)	0.0152(3)
Al1	0.2222	0.0876(6)	0.3447(3)	0.5	0.0152(3)
Al2	0.2222	0.1625(4)	0.4823(7)	0.2108(2)	0.0152(3)
O1	1.0	0	0.2579(1)	0.5	0.0167(1)
O2	1.0	0.1600(1)	0.3200(2)	0.5	0.0167(1)
O3	1.0	0.2604(1)	0.5208(3)	0.2373(5)	0.0167(1)
O4	1.0	0.1001(4)	0.4046(1)	0.3349(3)	0.0167(1)
O5	1.0	0.4269(2)	0.8537(4)	0.2763(4)	0.0167(1)
O6	1.0	0.1482(1)	0.4784(6)	0	0.0167(1)
K1	0.95	0.3333	0.6667	0.5	0.021(2)
K2	1.0	0	0.5	0.5	0.031(8)
K3	0.82	0	0.3000(4)	0	0.175(2)
K4	0	0	0	0	0.031(4)

a) Lattice constants are *a*= 13.3682 Å and *c*= 7.5258 Å, resulting in V= 2198.9 $Å^3$. The fit parameters are GOF=2.16, R_{wp}=5.63.

Table S4. Atomic parameters resulting from the Rietveld refinement of LTL-1[a]

Atom	Occupancy	*x*	*y*	*z*	U_{iso} (Å^2)
Si1	0.7777	0.0904(4)	0.3517(6)	0.5	0.0123(4)
Si2	0.7777	0.1632(2)	0.4880(5)	0.2076(4)	0.0123(4)
Al1	0.2222	0.0904(2)	0.3517(6)	0.5	0.0123(4)
Al2	0.2222	0.1632(4)	0.4880(1)	0.2076(2)	0.0123(4)
O1	1.0	0	0.2681(3)	0.5	0.0171(3)
O2	1.0	0.1656(4)	0.3313(9)	0.5	0.0171(3)
O3	1.0	0.2591(1)	0.5183(3)	0.2560(9)	0.0171(3)
O4	1.0	0.1027(4)	0.4085(8)	0.3306(2)	0.0171(3)
O5	1.0	0.4149(3)	0.8298(6)	0.2750(1)	0.0171(3)
O6	1.0	0.1414(3)	0.4810(2)	0	0.0171(3)
K1	0.93	0.3333	0.6667	0.5	0.023(3)
K2	0.98	0	0.5	0.5	0.024(2)
K3	0.81	0	0.2942(2)	0	0.172(3)
K4	0.09	0	0	0	0.081(1)
C1[b]	0.05	0.2201(2)	0.0843(1)	0.8590(4)	0.0215(4)
C2	0.05	0.2138(2)	0.0049(1)	0.9290(1)	0.0215(4)
C3	0.05	0.1201(2)	0.8651(1)	0.9960(8)	0.0215(4)
C4	0.05	0.0343(3)	0.7910(2)	0.9600(7)	0.0215(4)
C5	0.05	0.8992(4)	0.7268(6)	0.0710(9)	0.0215(4)
C6	0.05	0.8309(4)	0.7413(6)	0.1423(4)	0.0215(4)
C7	0.05	0.7353(3)	0.7818(7)	0.0491(5)	0.0215(4)
C8	0.05	0.7240(3)	0.8373(2)	0.9200(5)	0.0215(4)
C9	0.05	0.7850(4)	0.9805(3)	0.8431(4)	0.0215(4)
C10	0.05	0.8190(5)	0.0637(6)	0.9360(6)	0.0215(4)
C11	0.05	0.9387(5)	0.1654(7)	0.0820(5)	0.0215(4)
C12	0.05	0.0204(3)	0.1830(3)	0.1650(4)	0.0215(4)
C13	0.05	0.1560(2)	0.2160(3)	0.0913(5)	0.0215(4)
C14	0.05	0.2060(2)	0.1959(5)	0.9520(3)	0.0215(4)
Oo1[b]	0.05	0.1764(5)	0.1093(6)	0.9734(3)	0.0131(3)
Oo2	0.05	0.1309(3)	0.9386(3)	0.9143(3)	0.0131(3)
Oo3	0.05	0.9735(5)	0.8036(6)	0.0460(7)	0.0131(3)
Oo4	0.05	0.8102(2)	0.7823(3)	0.0112(4)	0.0131(3)
Oo5	0.05	0.7810(7)	0.9209(2)	0.9660(3)	0.0131(3)
Oo6	0.05	0.9015(5)	0.0894(8)	0.9890(6)	0.0131(3)
Oo7	0.05	0.0736(7)	0.1860(2)	0.0303(2)	0.0131(3)

a) Lattice constants are *a*= 13.3477 Å and *c*= 7.5274 Å, resulting in V=2198.9 Å^3. The fit parameters are GOF=3.94, R_{wp}=6.52.

b) C and Oo indicate carbon and oxygen atoms of CE molecule, respectively. Space group of CE was adopted as *P*1.

Table S5. Atomic parameters resulting from the Rietveld refinement of LTL-2[a]

Atom	Occupancy	*x*	*y*	*z*	U_{iso} (Å^2)
Si1	0.7777	0.0905(4)	0.3505(3)	0.5	0.0133(7)
Si2	0.7777	0.1609(3)	0.4878(5)	0.2057(1)	0.0133(7)
Al1	0.2222	0.0905(4)	0.3505(3)	0.5	0.0133(7)
Al2	0.2222	0.1609(3)	0.4878(5)	0.2057(1)	0.0133(7)
O1	1.0	0	0.2670(2)	0.5	0.0211(5)
O2	1.0	0.1635(4)	0.3270(8)	0.5	0.0211(5)
O3	1.0	0.2557(4)	0.5114(8)	0.2480(7)	0.0211(5)
O4	1.0	0.1040(4)	0.4088(4)	0.3307(2)	0.0211(5)
O5	1.0	0.4283(3)	0.8566(6)	0.3086(5)	0.0211(5)
O6	1.0	0.1370(6)	0.4676(5)	0	0.0211(5)
K1	0.90	0.3333	0.6667	0.5	0.043(2)
K2	0.93	0	0.5	0.5	0.052(3)
K3	0.79	0	0.2927(4)	0	0.312(6)
K4	0.21	0	0	0	0.121(2)
C1[b]	0.18	0.2200(5)	0.0842(3)	0.8585(4)	0.0217(7)
C2	0.18	0.2137(7)	0.0049(4)	0.9290(0)	0.0217(7)
C3	0.18	0.1200(9)	0.8652(4)	0.9960(8)	0.0217(7)
C4	0.18	0.0342(3)	0.7920(2)	0.9550(7)	0.0217(7)
C5	0.18	0.8991(4)	0.7269(6)	0.0710(9)	0.0217(7)
C6	0.18	0.8305(4)	0.7411(7)	0.1412(4)	0.0217(7)
C7	0.18	0.7354(3)	0.7816(7)	0.0492(5)	0.0217(7)
C8	0.18	0.7250(3)	0.8373(2)	0.9170(5)	0.0217(7)
C9	0.18	0.7860(4)	0.9803(3)	0.8450(4)	0.0217(7)
C10	0.18	0.8191(5)	0.0636(6)	0.9345(6)	0.0217(7)
C11	0.18	0.9388(5)	0.1653(7)	0.0820(5)	0.0217(7)
C12	0.18	0.0205(3)	0.1824(3)	0.1654(4)	0.0217(7)
C13	0.18	0.1550(2)	0.2156(3)	0.0912(5)	0.0217(7)
C14	0.18	0.2050(2)	0.1955(4)	0.9615(5)	0.0217(7)
Oo1[b]	0.18	0.1763(3)	0.1094(3)	0.9735(4)	0.0102(5)
Oo2	0.18	0.1308(7)	0.9384(5)	0.9120(8)	0.0102(5)
Oo3	0.18	0.9736(4)	0.8037(7)	0.0460(8)	0.0102(5)
Oo4	0.18	0.8105(2)	0.7823(8)	0.0108(5)	0.0102(5)
Oo5	0.18	0.7810(4)	0.9208(3)	0.9661(7)	0.0102(5)
Oo6	0.18	0.9016(5)	0.0893(6)	0.9880(6)	0.0102(5)
Oo7	0.18	0.0735(2)	0.1850(4)	0.0298(5)	0.0102(5)

a) Lattice constants are *a*= 13.3478 Å and *c*= 7.5271 Å, resulting in V= 2194.4 Å^3. The fit parameters are GOF=6.40, R_{wp}=9.76.

b) C and Oo indicate carbon and oxygen atoms of CE molecule, respectively. Space group of CE was adopted as *P*1.

Table S6. Atomic parameters resulting from the Rietveld refinement of LTL-4[a]

Atom	Occupancy	*x*	*y*	*z*	U_{iso} (Å^2)
Si1	0.7777	0.0929(4)	0.3517(2)	0.5	0.0121(2)
Si2	0.7777	0.1652(5)	0.4932(7)	0.2088(4)	0.0121(2)
Al1	0.2222	0.0929(4)	0.3517(2)	0.5	0.0121(2)
Al2	0.2222	0.1652(5)	0.4932(7)	0.2088(4)	0.0121(2)
O1	1.0	0	0.2714(2)	0.5	0.0157(1)
O2	1.0	0.1602(1)	0.3204(2)	0.5	0.0157(1)
O3	1.0	0.2591(4)	0.5182(8)	0.2645(7)	0.0157(1)
O4	1.0	0.1108(7)	0.4139(6)	0.3356(4)	0.0157(1)
O5	1.0	0.4229(5)	0.8459(9)	0.2851(7)	0.0157(1)
O6	1.0	0.1482(5)	0.4757(9)	0	0.0157(1)
K1	0.79	0.3333	0.6667	0.5	0.033(1)
K2	0.81	0	0.5	0.5	0.034(3)
K3	0.75	0	0.2860(2)	0	0.193(1)
K4	0.75	0	0	0	0.091(3)
C1[b]	0.76	0.2201(5)	0.0844(7)	0.8590(4)	0.0256(8)
C2	0.76	0.2140(2)	0.0048(1)	0.9280(3)	0.0256(8)
C3	0.76	0.1201(2)	0.8651(3)	0.9950(6)	0.0256(8)
C4	0.76	0.0343(3)	0.7910(4)	0.9590(1)	0.0256(8)
C5	0.76	0.8992(1)	0.7267(5)	0.0720(4)	0.0256(8)
C6	0.76	0.8308(1)	0.7410(1)	0.1420(5)	0.0256(8)
C7	0.76	0.7353(1)	0.7814(5)	0.0490(7)	0.0256(8)
C8	0.76	0.7240(3)	0.8372(6)	0.9190(2)	0.0256(8)
C9	0.76	0.7850(4)	0.9804(5)	0.8430(4)	0.0256(8)
C10	0.76	0.8190(5)	0.0637(3)	0.9350(2)	0.0256(8)
C11	0.76	0.9387(2)	0.1655(7)	0.0830(4)	0.0256(8)
C12	0.76	0.0203(7)	0.1831(4)	0.1660(2)	0.0256(8)
C13	0.76	0.1560(1)	0.2160(3)	0.0910(2)	0.0256(8)
C14	0.76	0.2060(2)	0.1959(1)	0.9620(4)	0.0256(8)
Oo1[b]	0.76	0.1766(4)	0.1095(4)	0.9738(1)	0.0232(4)
Oo2	0.76	0.1310(6)	0.9384(8)	0.9130(1)	0.0232(4)
Oo3	0.76	0.9737(5)	0.8035(1)	0.0460(6)	0.0232(4)
Oo4	0.76	0.8104(2)	0.7822(3)	0.0110(3)	0.0232(4)
Oo5	0.76	0.7800(3)	0.9210(2)	0.9660(5)	0.0232(4)
Oo6	0.76	0.9015(9)	0.0895(4)	0.9888(2)	0.0232(4)
Oo7	0.76	0.0737(3)	0.1860(5)	0.0300(4)	0.0232(4)

a) Lattice constants are *a*= 13.3433 Å and *c*= 7.5287 Å, resulting in V= 2193.8 Å^3. The fit parameters are GOF=5.06, R_{wp}=8.29.

b) C and Oo indicate carbon and oxygen atoms of CE molecule, respectively. Space group of CE was adopted as *P*1.

Reference

(1) Brent, R.; Lobo, A. J. W.; Lewis, D. W.; Anderson, M. W. *J. Phys. Chem. C* **2010**, *114*, 18240.

(2) Lee, Y. J.; Lee, J. S.; Yoon, K. B. Synthesis of Long Zeolite-L Crystals with Flat Facets. *Micropor. Mesopor. Mater.* **2005**, *80*, 237.

(3) Ziafati, A.; Sabzevari, O.; Heravi, M. Facile and Rapid Synthesis of Some Crown Ethers under Microwave Irradiation. *Phosphorus, Sulfur Silicon Relat. Elem*. **2006**, *181*, 803.

(4) Marra, G. L.; Fitch, A. N.; Zecchina, A.; Ricchiardi, G.; Salvalaggio, M.; Bordiga, S.; Lamberti, C. Cation location in dehydrated Na−Rb−Y Zeolite: An XRD and IR study. *J. Phys. Chem. B* **1997**, *101*, 10653-10660.

(5) Rietveld, H. M. The Rietveld method-A historical perspective. *Aust. J. Phys.* **1988**, *41*, 113-116.

(6) Petříček, V.; Dušek, M.; Palatinus, L. The crystallographic computing system JANA2006, Institute of Physics of the ASCR: Prague, Czech Republic, 2006.

(7) Barrer, R. M.; Villiger, H. Z. The Crystal Structure of the Synthetic Zeolite L. *Cryst. Mater.* **1969**, *128*, 352-370.

(8) Newsam, J. M. Structures of Dehydrated Potassium Zeolite L at 298 and 78 K and at 78 K Containing Sorbed Perdeuteriobenzene. *J. Phys. Chem.* **1989**, *93*, 7689.

(9) Burton, A.; Lobo, R. F. The Role of Barium Cations in the Synthesis of Low-silica LTL Zeolites. *Microporous Mesoporous Mater.* **1999**, *33*, 97.

(10) Anderson, P. A.; Armstrong, A. R.; Porch, A.; Edwards, P. P.; Woodall, L. J. Structure and Electronic Properties of Potassium-Loaded Zeolite L. *J. Phys. Chem. B* **1997,** *101,* 9892.

(11) Henderson, R; Moffat, J. K. The Difference Fourier Technique in Protein Crystallography: Errors and Their Treatment. *Acta Crystallogr. B* **1971**, *27*, 1414-1420.